batteries

MDPI

Article

Analysis and Investigation of Thermal Runaway Propagation for a Mechanically Constrained Lithium-Ion Pouch Cell Module

Luigi Aiello [1,*], Ilie Hanzu [2,3], Gregor Gstrein [1], Eduard Ewert [4], Christian Ellersdorfer [1] and Wolfgang Sinz [1]

1 Vehicle Safety Institute, Graz University of Technology, Inffeldgasse 23/I, 8010 Graz, Austria; gregor.gstrein@tugraz.at (G.G.); christian.ellersdorfer@tugraz.at (C.E.); wolfgang.sinz@tugraz.at (W.S.)
2 Institute for Chemistry and Technology of Materials, Graz University of Technology, (NAWI Graz), Stremayrgasse 9, 8010 Graz, Austria; hanzu@tugraz.at
3 Alistore—ERI European Research Institute, CNRS FR3104, Hub de l'Energie, Rue Baudelocque, 80039 Amiens, France
4 Dr. Ing. h.c. F. Porsche Aktiengesellschaft, Porschestr. 911, 71287 Weissach, Germany; eduard.ewert@porsche.de
* Correspondence: luigi.aiello@tugraz.at; Tel.: +43-(316)-873-30367

Abstract: In this paper, tests and analysis of thermal runaway propagation for commercial modules consisting of four 41 Ah Li-ion pouch cells are presented. Module samples were tested at 100% state-of-charge and mechanically constrained between two steel plates to provide thermal and mechanical contact between the parts. Voltage and temperature of each cell were monitored during the whole experiment. The triggering of the exothermal reactions was obtained by overheating one cell of the stack with a flat steel heater. In preliminary studies, the melting temperature of the separator was measured (from an extracted sample) with differential scanning calorimetry and thermogravimetric analysis techniques, revealing a tri-layers separator with two melting points (≈135 °C and ≈170 °C). The tests on module level revealed 8 distinct phases observed and analyzed in the respective temperature ranges, including smoking, venting, sparkling, and massive, short circuit condition. The triggering temperature of the cells resulted to be close to the melting temperature of the separator obtained in preliminary tests, confirming that the violent exothermal reactions of thermal runaway are caused by the internal separator failure. Postmortem inspections of the modules revealed the internal electrical failure path in one cell and the propagation of the internal short circuit in its active material volume, suggesting that the expansion of the electrolyte plays a role in the short circuit propagation at the single cell level. The complete thermal runaway propagation process was repeated on 5 modules and ended on average 60 s after the first thermal runaway triggered cell reached a top temperature of 1100 °C.

Keywords: thermal runaway; propagation analysis; thermal trigger; overheating; lithium ions batteries; internal short circuit; gas venting; differential scanning calorimetry

check for updates

Citation: Aiello, L.; Hanzu, I.; Gstrein, G.; Ewert, E.; Ellersdorfer, C.; Sinz, W. Analysis and Investigation of Thermal Runaway Propagation for a Mechanically Constrained Lithium-Ion Pouch Cell Module. *Batteries* **2021**, *7*, 49. https://doi.org/10.3390/batteries7030049

Academic Editor: Carlos Ziebert

Received: 31 May 2021
Accepted: 13 July 2021
Published: 19 July 2021

Publisher's Note: MDPI stays neutral with regard to jurisdictional claims in published maps and institutional affiliations.

Copyright: © 2021 by the authors. Licensee MDPI, Basel, Switzerland. This article is an open access article distributed under the terms and conditions of the Creative Commons Attribution (CC BY) license (https://creativecommons.org/licenses/by/4.0/).

1. Introduction

Propagation speed of thermal runaway (TR) in a Li-ion battery module is an important phenomenon to consider as part of the battery pack design process. In fact, the timing between a first detectable TR event and a battery pack hazardous condition needs to be conformal to homologation requirements [1]. Testing a single module opportunely triggered in TR condition can be useful to understand the propagation process before scaling it on battery pack level. Since TR exothermal behavior can differ based on the triggering methods, a research about the initiation of TR was conducted. As found in literature, a Li-ion cell failure can result from a variety of abuse conditions: mechanical, electrical, thermal, or manufacturing defects [2–8]. In general, the exothermal behavior of the TR can change if the cell is triggered under different abuse conditions [9–13]; as a

consequence, the initiation of TR is a fundamental aspect to consider to obtain test results in the direction of the desired target. On the module level, if the TR is triggered in a first cell, this will start exothermal reactions, causing thermal and mechanical stress to the adjacent cells and likely propagating with a cascade process involving multiple cells, or, in worst case, the whole module [11,14–19]. Considering the aforementioned, if the TR propagation speed needs to be analyzed in a Li-ion cells module, since the triggering method affects the exothermal behavior of the first cell, it must be carefully chosen since it could affect the propagation speed. In fact, if the initiation is induced externally, for example, by a mechanical actuator (i.e., nail penetration), its exothermal behavior could be very different with respect to the next triggered cells (induced by cascade effect), likely also causing a difference in propagation velocity. Since the aim of this study is the TR propagation speed, the triggering method must reproduce, as close as possible, the stress and abuse loads that a cell in TR applies to the adjacent ones during the cascade effect. Furthermore, the triggering method must be robust and exhibit good repeatability.

In the literature, several methods were found to initiate TR in a system with multiple Li-ion cells, however, all the investigated procedures can be reclassified into three main cases: object penetration [14], external heating [9,11,15,17–19], or electrical overcharge [20,21]. In general, the overheating of the Li-ion cell can be obtained by an external thermal source or by an abusive electrical operation, i.e., forcing an electric current and/or voltage above the nominal values. For example, in Cheng et al. [9], the thermal runaway is triggered using a suitable heater placed at the center of the prismatic cells stack. This initiates the TR by overheating the central cells. In this case, the heater must be chosen of the same size of the cell surface and power must be enough to reach a TR state. Instead, Feng et al. [14] utilizes a sharp object to penetrate the first cell of the stack, thus initiating the TR not in the center but on the side of the stack. Electrical overcharging can also push a Li-ion cell to TR, as indicated in Sun et al. [20]; however, since the state of charge (SOC) is a parameter that affects the TR behavior [22–27], this triggering method would not be preferred if the desired outcome is the exothermal behavior of the module. The overheating can also be obtained by the electrical induction phenomenon. Since the battery housing is generally made of steel/aluminum, an excitation electrical current can be induced on it with an external electromagnetic field [13].

Based on the conducted literature research, a test design was developed for the evaluation of TR propagation in Li-ion pouch cell module. The proposed test concept allows mechanical constraint to be applied on the cell stack and to precisely measure the amount of heat introduced in-to the system, thus evaluating the amount of energy for TR activation. The samples of pouch Li-ion battery modules were obtained from a commercialized battery pack of an all-electric vehicle. Module description is reported in Section 2.1. Further details of the battery pack, modules, chemistry and internal materials are reported in publication Kovachev et al. [28]. The experiment presented in this manuscript was conducted to evaluate the speed of thermal runaway propagation between pouch cells in a commercial Li-ion battery module. The produced data on module level can be utilized for validation of simulation models and then further extended for battery pack simulations.

2. Experimental

The aim of the experiment was to obtain more insights into TR of a single cell and TR propagation, as well as suitable input data for simulation purposes. The TR of the first cell was triggered by overheating the cell at the bottom of the cell stack. The novelty of the test setup is the triggering method: a custom flat steel heater—connected to a high power electrical supply—positioned at the bottom of the cell stack allowed to provide controlled heat and, concurrently, to constrain the stack in between two steel plates. The heater was produced with laser cut technology from 1 mm steel foil; it was then possible to fulfill minimum power requirements and to fit the battery cell surface for a homogeneous heat distribution. Voltage and current provided to the heater were constantly monitored during the experiment allowing to monitor the amount of heat introduced into the system. The

module, composed by four Li-ion pouch stacked cells was placed in between the two steel plates to constrain the cells during the whole test. A sketch of the assembly is reported in Figure 1.

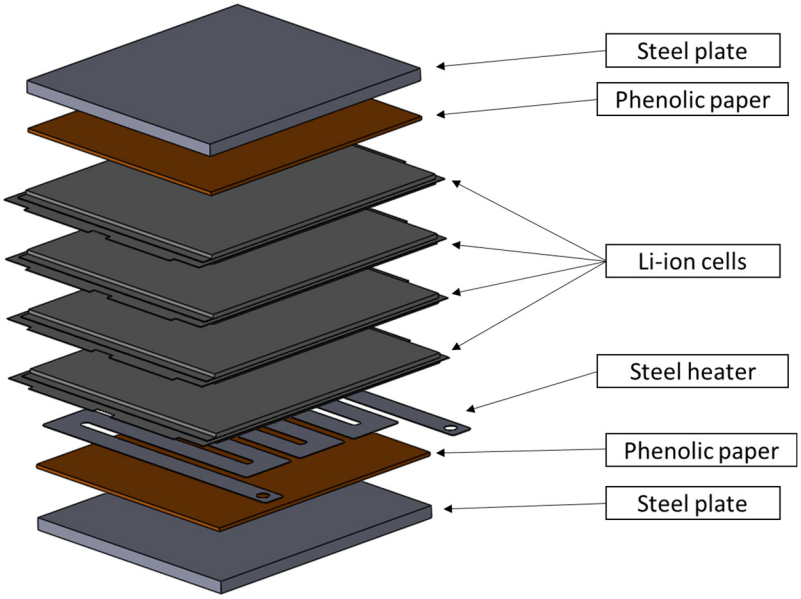

Figure 1. Parts concept description of test assembly for thermal runaway propagation test. Flat heater at bottom of stack is meant to trigger first cell without affecting mechanical compression in stack.

The steel plates were bolted to each other at minimum pressure to guarantee thermal contact between the parts and a displacement constraint. Thermocouples were placed in strategic points—at the very top and bottom of the stack, and in between every cell—and applied with aluminum thermal paste to make a better thermal contact with the part. As indicated in Figure 1, two plates of phenolic paper were sandwiched between the steel plates of the stack. There are two reasons for this: the first is to separate the cell stack from the steel plates to avoid strong thermal losses, the second is to guarantee electrical insulation of the steel heater from the steel plate.

2.1. Samples Description

The Li-ion cell module samples were obtained from an all-electric vehicle which was commercialized in 2016. Each module contained a stack of four Li-ion pouch cells glued together on the surface of the central contact area and kept in place by an external plastic/silicon frame. The four holes in the plastic frame were made to receive four steel cylinders for reasons of mechanical constraint. Furthermore, the cells were connected with a 2p2s electrical configuration: the tabs were welded on three copper step-shaped bars ending with three output terminals. The single cells were laminated pouch-type with a rated capacity of 41 Ah and a nominal voltage of 3.7 V. The chemistry of the electrodes was determined by an analytic cell dissection, as described in the publication of Kovachev et al. [28]. The cathode chemistry is a spinel of NMC and LMO, and the anode electrode is made of Graphite. Each cell had a weight of approximately 800 g with a size of 290 mm $\times$ 216 mm $\times$ 8 mm. Pictures of the module and its tabs connections are reported in Figure 2.

Four resin spots were found at the four corners of each cell with the purpose of fixing the plastic frames to the cells themselves, and in correspondence of the resin spots, the external pouch of the cells were presenting holes of 3 mm diameters. While dismantling, the silicon edges showed some resistance when pulled apart; this was probably due to a thin layer of glue placed all around the frame.

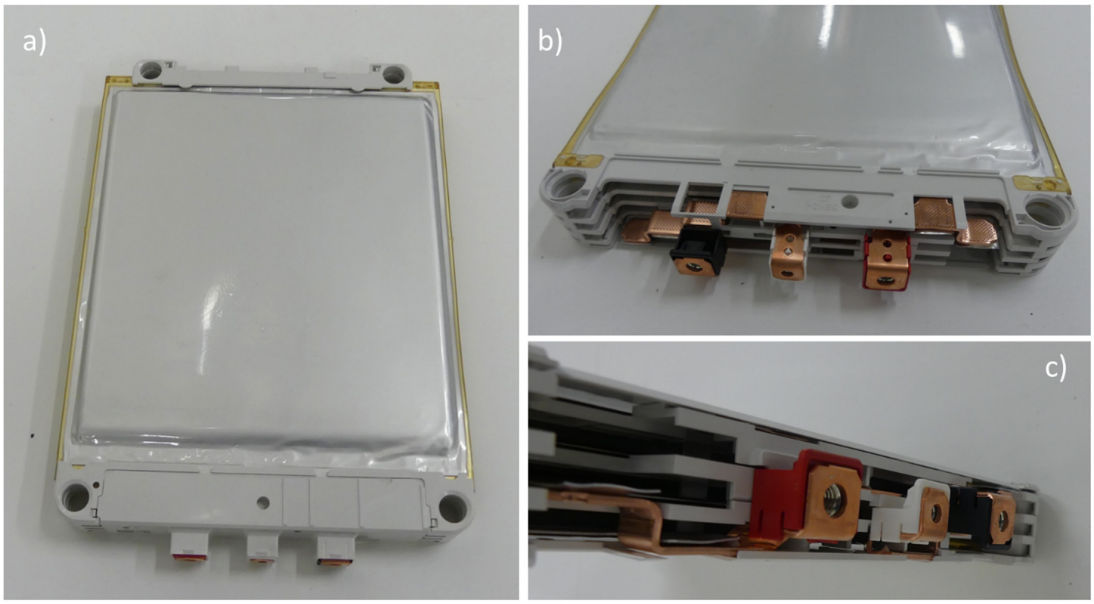

Figure 2. (**a**) Module sample used for test is composed of four cells stacked and glued to each other; each cell is surrounded by a plastic-silicon frame; (**b**) Top view of copper busbars: cells are electrically connected in the 2s2p configuration; (**c**) Detail of the connection busbars of module.

2.2. Samples Preparation

The modules were prepared preserving the manufacturer's glue between the cells to guarantee that the thermal contact cell-to-cell was optimal. At first, the modules were set to 100% SOC with a standard procedure: a charging current was applied at 1-C rate (82 A), and once the charging device switched to Voltage Control mode, the procedure was ended when electrical current was below the C/20 C-rate. The SOC setting was carried out with a programmable DC power supply (Model: EA-PSI 9000 3U), an electronic load (Model: EA-EL 9000 B), and a coulomb counter implemented with a precision DC Current Transducer (Model: CT-1000). The modules included frames made of plastic and silicon materials glued directly to the pouch bag edges of each cell. The frames were clearly added by the manufacturer to ensure the cells alignment and avoid undesired contacts between the busbars and/or current collectors. Since those plastic frames were external to the active material area, they were considered not relevant for the cell-to-cell heat conduction; hence, the frames were removed with a special disassembling procedure. The steps and tools utilized for the module preparation are shown in Figure 3.

To separately monitor the electric voltage of each cell, the electric busbars connections needed to be removed before proceeding with the test setup.

At first, the accessible busbars connections were cut with a ceramic knife; then, the four resin spots (as illustrated in Figure 3b) were removed with a 3 mm drill bit. At this point, the first plastic frame could be detached with a minimum pullout force, and the next tabs became accessible to advance with the preparation procedure.

2.3. Equipment and Sensors

The heater was built from a 1 mm steel foil suitably shaped by laser cutting and it was electrically supplied with the same programmable DC power supply used for the SOC setting (power supply: EA-PSI 9000 3U). Voltage and current provided to the heater were measured during the whole experiment to evaluate the heat power introduced into the system. The heater was designed to obtain the required heating power and to fit the sizes of the battery. Voltages and temperatures (captured with type K thermocouples) were measured at 2 kHz with NI expandable data logger (cDAQ-NI 9178). The electric current was measured with a precision electric current transducer (model: CT-1000) from FLUCS company.

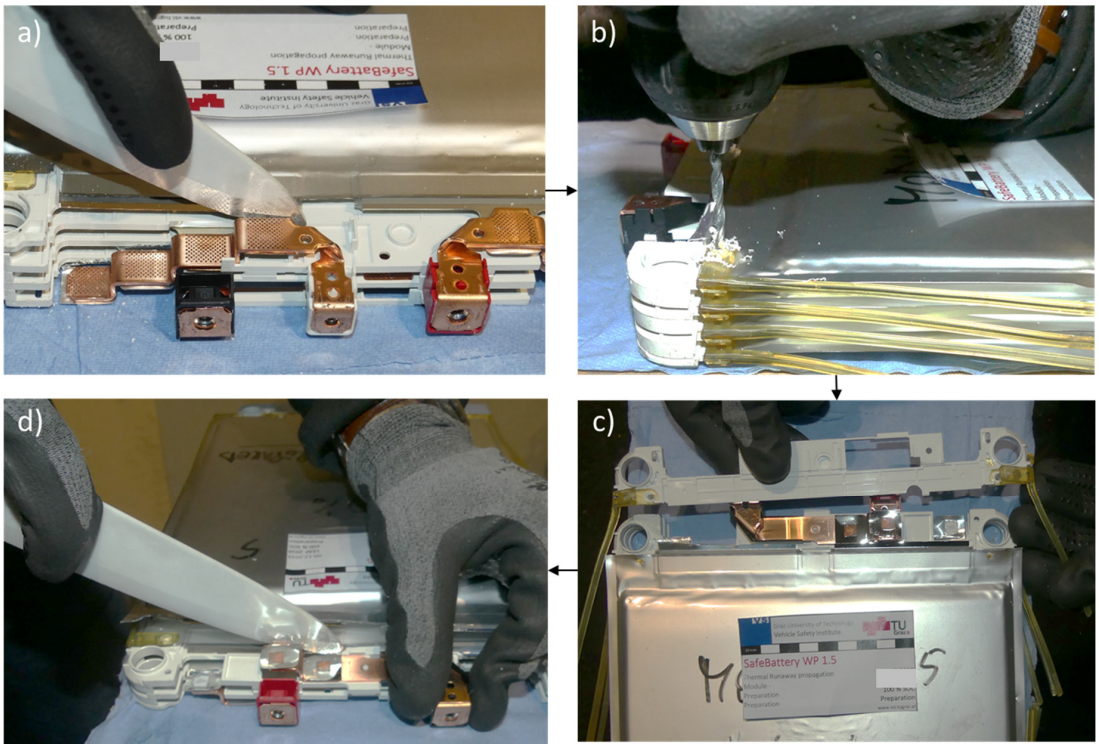

Figure 3. Procedure for partial disassembling of Li-ion cell module. (**a**) First two levels of accessible busbars are removed with a ceramic cutter; (**b**) Resin spots of first two cells are removed with a 3 mm drill bit; (**c**) Plastic frames are removed uncovering next busbars layers; (**d**) Procedure is repeated for further busbars layers.

2.4. Test Setup and Procedure

Thermocouples were positioned to obtain meaningful information regarding the propagation of TR, hence the temperature sensors were placed between each cell as well as at the top and bottom of the stack, as described in Figure 4. As illustrated, since the original glue between the cells was preserved, the thermocouple numbers 2, 3, and 4 could not be placed in the center of the stack but just at the edge of the internal glued surface.

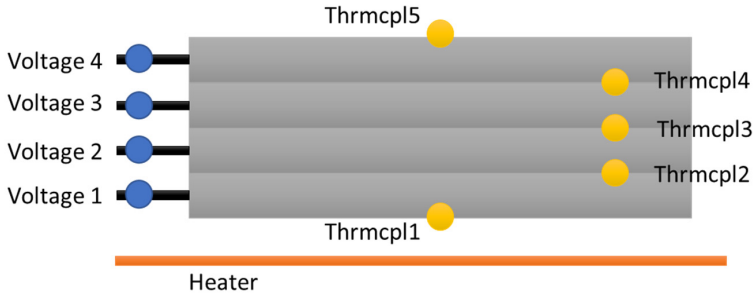

Figure 4. Description of sensors' positioning for TR propagation experiment. Thermocouples 2,3 and 4 could not be placed on same vertical axis of thermocouples 1 and 5 since manufacturer's glue was preserved. Therefore, middle area between cells was not accessible.

The triggering of TR was performed by providing an electric current to the heater described in Section 2.3 with the target power of 600 W, provoking a temperature increase of about 2 °C/min. When threshold temperature was reached a visible increase of temperature occurred, then the electric current was manually interrupted by the operator. The experiments were conducted outdoors and recorded with a digital camera that was activated just a few minutes before the TR critical temperature was reached. Furthermore, an additional surveillance camera (remotely controlled) was put in place to allow the operators to detect smoke and fire in real time and manually deactivate the heater when

TR started. A blower was positioned at approximately two meters from the module to flush away smoke during the TR, this device was active during the whole test duration. A total of five repetitions were conducted with the aim to increase the chances of observing a common behavior of TR and its propagation. Since the TR behavior is usually violent—due to extreme gas venting and high temperatures—loss of contact of the temperature sensors or voltage cables in some tests was considered possible.

2.5. Analysis of the Separator with Differential Scanning Calorimeter

Since thermal runaway threshold temperature mainly depends on the separator softening/melting temperature [3,4,9,10], the separator material of the Li-ion cells under analysis was investigated. The exothermal/endothermal behavior of the separator was investigated by simultaneous thermal analysis (STA) that provided information on both mass loss and heat flow. The instrument used was STA 449C Jupiter from "NETZSCH". The temperature program consisted of a temperature ramp from 20 °C to 550 °C at a heating rate of 10°/min. Al2O3 (alumina) crucibles were used, and the atmosphere was helium.

The preparation of the samples for the DSC analysis was done disassembling a battery in the glovebox and cutting 5 mm disks out of the separator layer. During the extraction, most of the electrolyte vaporized and got lost; however, the samples were sealed immediately in a small aluminum container. In the results, the effect of the residual electrolyte is well-visible in the expected temperature range.

3. Results

3.1. DSC Analysis of Separator

The aim of this measurement is the determination of materials phase change temperatures; in particular, the melting temperature of the separator. In Figure 5 are shown the thermogravimetric analysis (TGA) and differential scanning calorimetry (DSC) curves of the separator as taken from the opened cell, with no solvent rinsing and after several days of storage under ambient atmosphere.

At temperatures between 50 and 200 °C, three endothermic peaks related to the separator can be seen. The process occurring at lower temperatures around 100 °C likely corresponds to the shrinking of the polyolefin part of the separator; water evaporation may also contribute in this temperature region.

The peaks centered at 134 °C and 170 °C very likely correspond to the melting point of different separator components such as polyethylene and polypropylene. The other endothermal and exothermal peaks can be explained taking into consideration that the separator was not rinsed with any solvent before analysis. Samples were simply taken from cell after disassembly with no further treatment. Consequently, the investigated separator contained a significant quantity of solvents, very likely those having a lower vapor pressure such as ethylene carbonate (EC), as well as some lithium hexaflourophosphate (LiPF6) salt. The other two components of the solvent mixture, namely diethyl carbonate (DEC) and dimethyl carbonate (DMC), have high vapor pressures and are thus volatile. It is plausible to consider that DEC and DMC completely evaporated during the preparation for analysis and storage of the separator under ambient atmosphere for several days before measurements. Indeed, in Figure 5 we see an endothermic peak centered about 34–35 °C that very nicely fits to the melting temperature of crystalline EC embedded in the separator.

The endothermic peak centered at 134 °C can very likely be ascribed to the melting point of the polyethylene (PE) layer(s) in the separator, a phenomenon that is known to occur around 130 °C. Further on, the endothermic peak centered at 170 °C is characteristic to the melting point of polypropylene (PP) layer of the separator. This confirms that the separator is a multilayer separator, made of PE and PP each with slightly different mechanical and thermal properties and porous so that a liquid electrolyte can be retained in the separator and ensure ion conduction.

At temperatures above 250 °C, the LiPF6 salt is known to decompose exothermally into LiF and PF5, a reaction that matches very well the major endothermic peak around 270 °C.

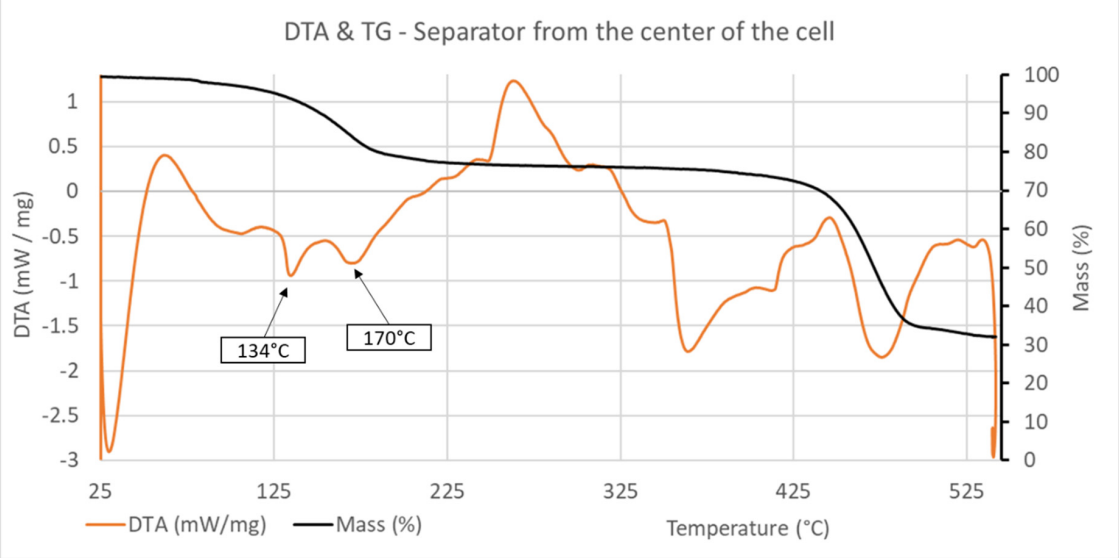

Figure 5. Thermogravimetric analysis (TGA) and differential scanning calorimetry (DSC) curves of separator as taken from opened cell, with no solvent rinsing and after several days of storage under ambient atmosphere.

3.2. Observable TR Phases

During the tests, we observed a sequence of phases in common for all the experiments and—for each step—identified the respective (externally measured) temperature ranges. The identified eight phases—associated to observable phenomena—were correlated to the expected physical processes occurring inside the cells and listed in Table 1. The eight phases described in Table 1 cannot be identified for each of the four cells of the stack; in fact, once the first cell was triggered, gas venting, and fire did not allow us to have a clear sight on the module. Furthermore, the speed of heat released from a triggered cell is certainly higher than the heating power of the steel heater, provoking a faster transition between phases for the successive cells, complicating the phases identification. Supplying the heater, the first cell of the stack was warmed-up at a rate of approximately 0.2 °C/s (measured on thermocouple 1) from ambient temperature until the TR trigger temperature was reached. At this temperature threshold, the temperature increase can be sustained by the self-heat generation of the cell but it does not correspond to the very first self-heating temperature; in fact, that would be related to the decomposition of the solid electrolyte interface (SEI) layer, occurring already from about 80–90 °C [4,10]. Adiabatic experiment must be performed to precisely observe this temperature threshold.

The self-heating rate due to this phenomenon (SEI decomposition) would be not enough to provide a visible temperature increase of the system and a further deeper TR state. The reason is that this test is not performed in an adiabatic condition: a cooling effect from the external environment is constantly present, requiring the external heating device to be active until higher temperature is reached.

Considering the above-mentioned, no visible effects were registered during the external warm-up phase until 170 °C (*phase 1*). In the range 170–190 °C (*phase 2*), a slight white smoke was detected, probably due to the electrolyte evaporation through the sealing; during this phase, impulsive and temporary increase of internal pressure were detected by observing slight movements and bending of the steel plates. As soon as *phase 3* started, the heater was turned off. A fast increase in temperature was detected as well as a strong movement of the steel plates, which indicates a strong increase in internal pressure that was certainly related to local internal short circuits due to mechanical failure of the separator, and in turn leads to the rupture of the pouch bag (*phase 4*). The breakdown of the pouch bag led to a consequent gas venting and drop of the internal pressure, and once hot gases are released to the surroundings with available oxygen, their combustion can be initiated

(*phase 5*). Local short circuits melt down small pieces of the current collectors (presumably the aluminum of the cathode current collector), thus generating flying burning embers that can potentially initiate the combustion of the vented gases. In every repetition test, combustion of the vented gases always occurred, so that a *phase 6* was specially introduced to define this event. Since all the events were recorded by a high definition camera, in Figure 6 are reported the frames relative to the beginning of each phase described in Table 1. The violent exothermal reaction phase is followed by a slower heat generation condition; this is indicated by *phase 7*, where uncombusted active materials are still present, decomposing gradually and fading to a passive cooling condition. In this phase, small regions of the active material could be still functioning, thus presenting a fading exothermal behavior. Once all the parts are combusted, the system enters *phase 8*: during this last phase, the system cools slowly down to ambient temperature.

Table 1. Description of TR phases and their observable phenomena and respective external temperature ranges.

	Observable Phenomena	Temperature Range (External)
Phase 1	No visible effect	<170 °C
Phase 2	Slight smoke release, possible electrolyte leakage, impulsive and discontinuous increase of internal pressure	170–190 °C
Phase 3	Fast swelling, fast increase of internal pressure and temperature	190–220 °C
Phase 4	Pouch bag opens, gas venting, decrease of internal pressure, decompression could cause instantaneous temperature drop	>220 °C
Phase 5	Gas venting, sparks initiate the combustion of vented gas	>220 °C
Phase 6	Deep short circuit and gas combustion, triggering of next cells	-
Phase 7	Rise of temperature and pressure is over, system starts to decrease its temperature, uncombusted materials are still present	-
Phase 8	All active materials are combusted, system cools down slowly	-

The described TR phases were observed for all the five experiments performed; temperatures and voltages were monitored and reported in the next sections.

3.3. Temperature Measurements

The position of the sensors were described in Figure 4, five thermocouples were positioned at every layer of the stack (in between the cells) to obtain the temperature gradients in TR propagation direction. Thermocouples are numbered in such a way that the higher the number, the higher the distance from the heater (as illustrated in Figure 4 and consequently—during TR events—the temperatures of the thermocouples increased according to the numbering order. In some cases—due to violent gas venting—thermocouples were losing contact with the parts (temporary or for the rest of the experiment), with consequent loss of temperature data. Regarding the experiments described in this study, two of five tests showed partial loss of data, although the lost data could be reconstructed by interpolation. For results demonstration just one experiment will be considered, and the temperature results of the other tests can be found in the Appendix A. Plots of the recorded temperatures—overview and zoom on TR propagation—are illustrated in Figure 7.

Analysis of TR propagation speed can be carried out from the temperature data of Figure 7b: it is possible to observe the trigger temperature from *Thrmcpl 1* (the one closest to the heater) of about 200 °C. Furthermore, referring to the same temperature curve (*Thrmcpl 1*), a small negative peak is present just before the temperature rise, corresponding to the main gas venting event. This peak is not present on the next 4 thermocouples when TR is triggered. The two thermocouples *Thrmcpl 3* and *Thrmcpl 4* reach a higher temperature with respect to the others. The reason can be addressed to the thermocouples position: since they are placed internally to the stack, there is less heat exchange with the surroundings during the experiment.

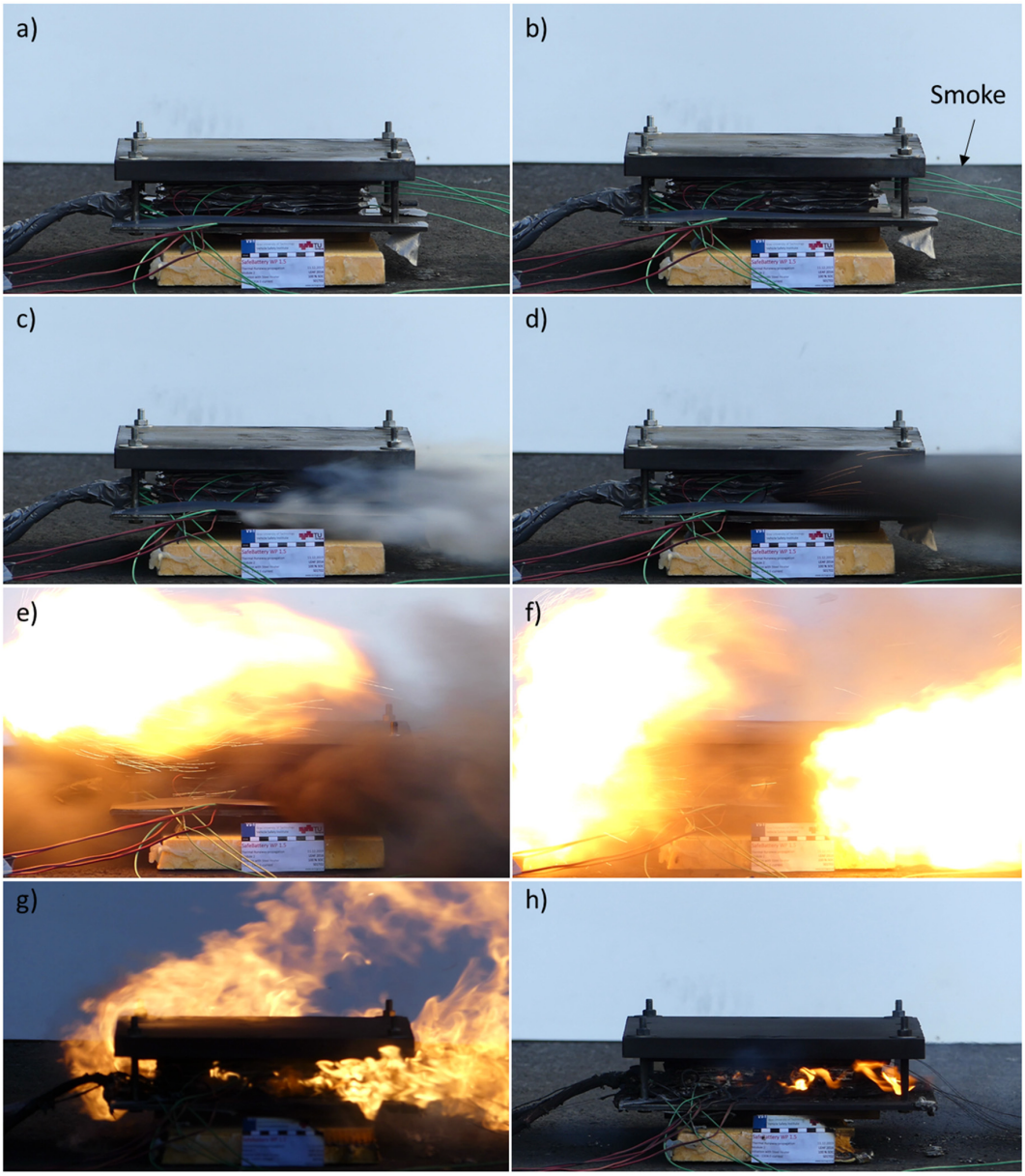

Figure 6. Description of the TR phases observed and recorded with a high-definition camera: (**a**) initial warm up phase, no observable effects; (**b**) slight smoke detected, probably due to electrolyte evaporation through sealing; (**c**) gas venting, sparks and embers are not yet present, smoke is mainly of white color; (**d**) gas venting with increased speed, gas has a darker color, sparkles and embers occur; (**e**) due to sparkles and embers, vented gas initiate combustion; (**f**) deep TR and combustion of vented gases; (**g**) system starts to cool down, uncombusted active materials are still present and burning slowly; (**h**) active materials are all combusted, system cools down.

3.4. Voltage Measurements

Since the violent exothermal behavior of TR is mainly triggered by the internal electrical short circuit [4,10], voltage measurements of the cells provide a more precise information regarding the TR triggering time and propagation. The external temperature rise—monitored by temperature sensors—is an effect occurring with a certain time delay with respect to the internal electrical short circuit.

Plotting the temperature and voltage data, this phenomenon and the related delay, which in this case was approximately 3 s (as shown in Figure 8), are observable.

Figure 9 shows the voltages of the 4 cells in the thermal runaway time window for the test carried out on "Module 2". It is possible to observe several small peaks on the voltage

curves (in particular cell numbers 3 and 4), those peaks are due to the instability of the internal short circuit brought about during the warmup phase. In Figure 9 at time ≈ 900 s, a massive short circuit occurs in cell number 1. After 12 s, the cell number 2 is triggered, also exhibiting a faster transition to massive short circuit compared to cell 1. In the same plot (i.e. Figure 9) a difference in terms of propagation time and severity of the internal short circuit—by a more gentle discharging curve—can be observed for cells 3 and 4. This difference can be attributed to the different stack pressure status when cell 3 and 4 are triggered. Once cell 1 and cell 2 initiated TR and vented gas, the internal stack pressure drops.

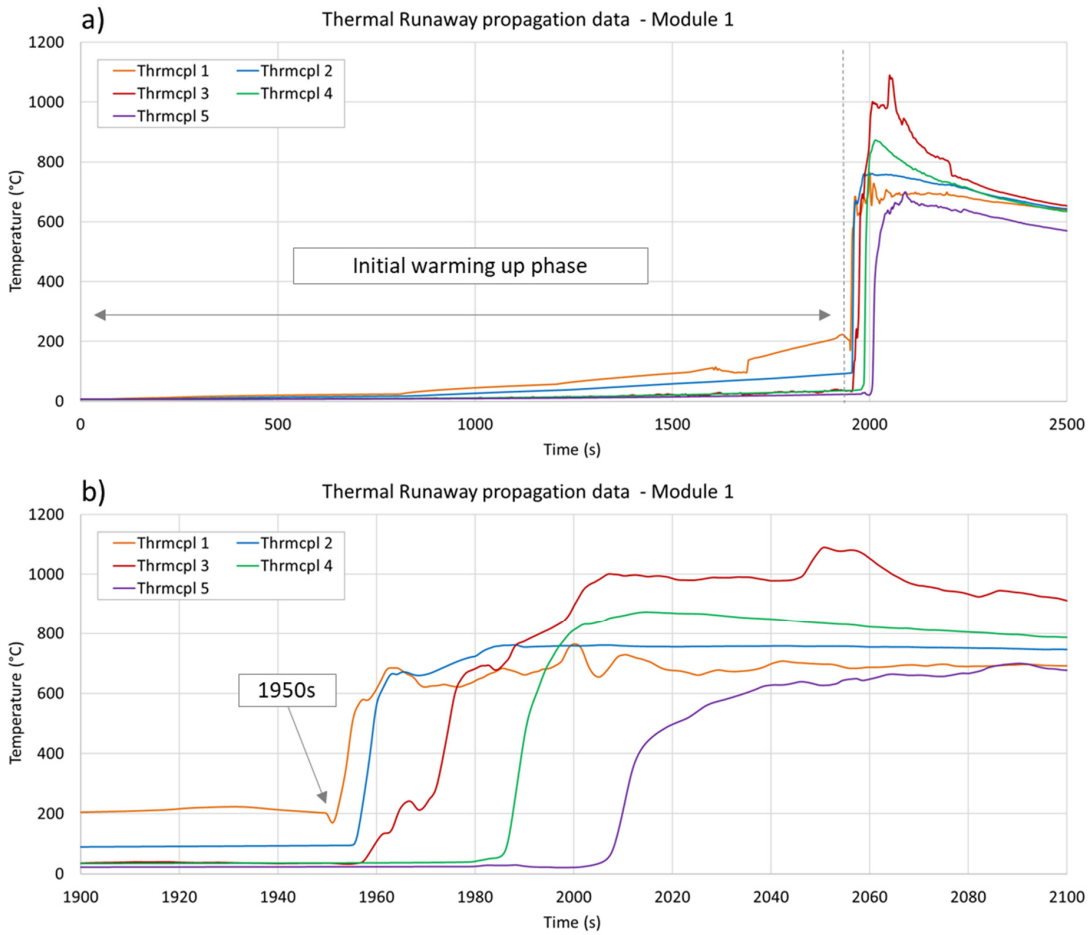

Figure 7. Plots of temperatures recorded by the 5 thermocouples for TR propagation test; (**a**) Overview of 5 temperature sensors; time window is set from beginning to end of experiment; (**b**) Zoom of time window where temperatures rise in correspondence to TR.

A comparison of the triggering time of the 5 tested modules—regarding the voltage drop behavior—is reported in Table 2. In some cases, it was not possible to derive the TR initiation time; this is indicated in the table as "Loss of Contact" (LoC). Appendix A shows the temperature and voltage measurement curves for each conducted test.

The heating power was manually regulated by the operator and turned off when TR was visibly triggered by temperature observation (as illustrated in phase three from Table 1). For this reason, the triggering time is different in each test.

3.5. Postmortem Inspection

After the completion of the experiments, the modules were inspected to find possible evidence to confirm the steps and phases observed and recorded during the experiment. Evidence of internal short circuit and triggered active material were found by removing

the pouch bag from the top cell of the stack, thus clearly revealing that the propagation of the short circuit was due to local pressure increase as consequence of short circuit initiation. Referring to cell number 4 (the cell at the top of the stack) of the tested module 2, the sign of initial short circuit and consequent propagation was significant, as reported in Figure 10.

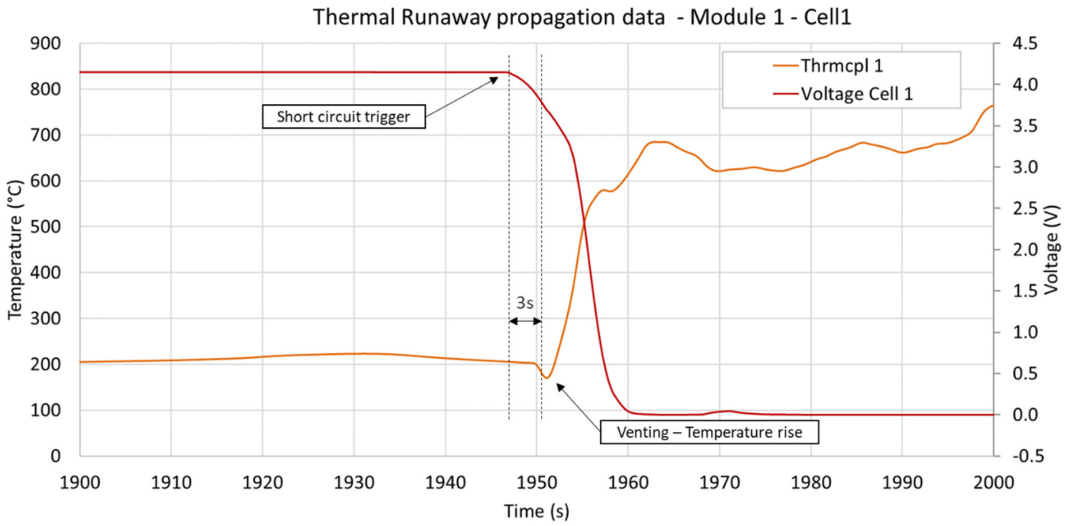

Figure 8. Comparison of temperature and voltage for cell 1 triggered to TR condition. Time between short circuit and temperature rise is approximately 3 s.

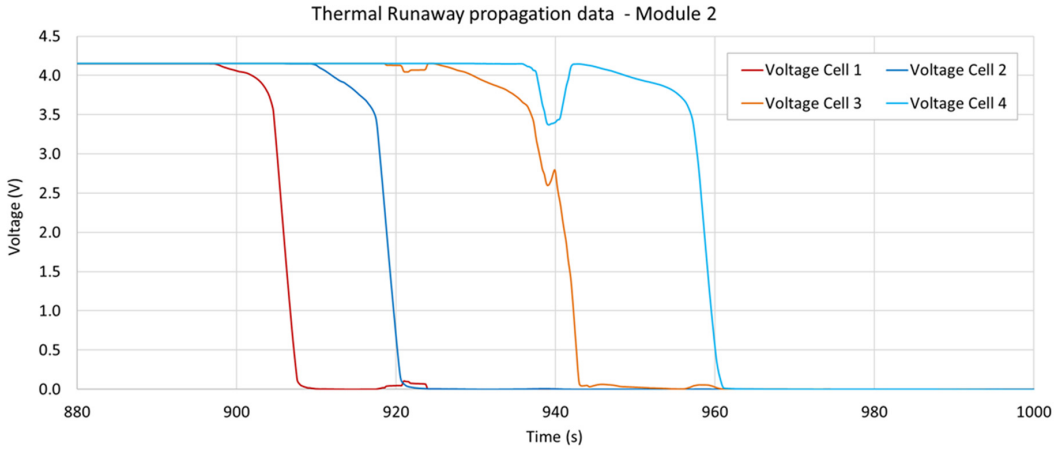

Figure 9. Voltage behavior of cells after trigger of TR. First cell exhibits a faster transition in deep thermal runaway indicating a more severe electrical short circuit condition. After venting of the first cell, stack pressure decreases reducing electrical short circuit severity for successive cells. Discontinuities of voltages for cells 3 and 4 are due to venting of adjacent cells.

Table 2. TR propagation times based on the voltage drop measurements. Some values are missing—indicated as: Loss of Contact (LoC)—since cables contacts were lost during test due to violent gas venting.

TR Triggering Propagation Time—Based on Voltage Drops				
	Cell 1	**Cell 2**	**Cell 3**	**Cell 4**
Module 1	1947.4 s	1958.8 s (+11.4)	LoC	LoC
Module 2	897.9 s	909.9 s (+12.0)	924.4 s (+14.5)	941.9 s (+17.5)
Module 3	660.5 s	LoC	LoC	LoC
Module 4	1157.4 s	1168.3 s (+10.9)	1184.4 s (+16.1)	1203.1 s (+18.7)
Module 5	1045.3 s	1051.1 s (+5.8)	1062.3 s (+11.2)	1075.0 s (+12.7)

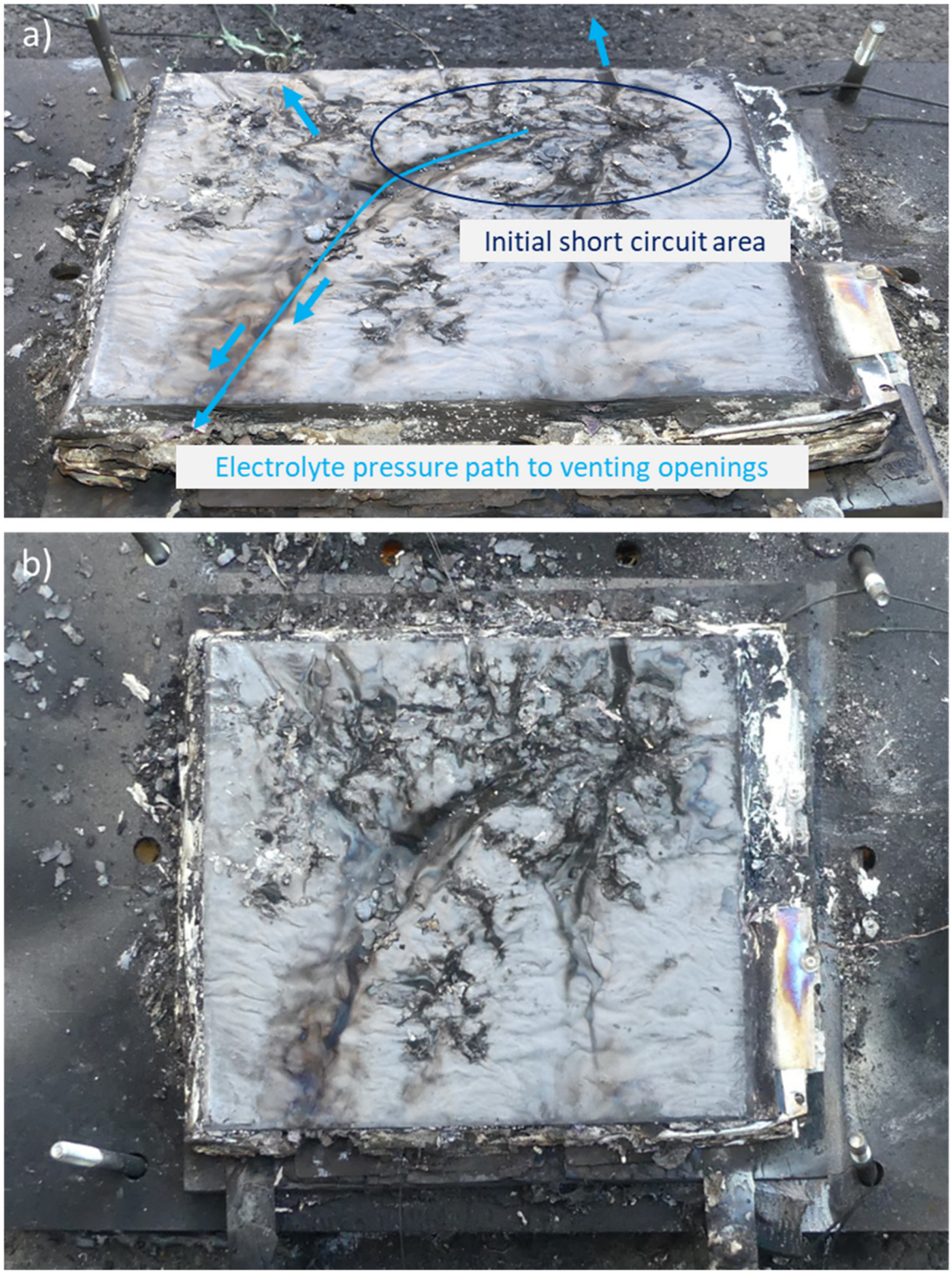

Figure 10. Inspection of battery module after test completion (**a**) Perspective view (**b**) Top view. Traces of burned material on the path of internal short circuit and high temperature electrolyte are well visible on top layer.

Looking at Figure 10, it is possible to make assumptions about the process of internal short circuit and its propagation during TR. As the first short circuit is triggered, the electrolyte warms up quickly and expands in its surrounding, thus triggering mechanical stress on the adjacent layers leading to an avalanche effect. The short circuit propagates with branching shape until it reaches the cell edges, as shown in Figure 10. A sketch to illustrate how this phenomenon can take place on single layer level is shown in the results discussion section.

4. Results Discussion

The presented data and postmortem inspection can be analyzed to make assumptions regarding the electrothermal behavior of the cells when internal failure occurs. When thermal stress is applied (by the external heater) at a certain temperature, the separator loses its mechanical stability. This temperature threshold can be estimated from the melting point obtained by DSC analysis (as illustrated in Figure 5). In Figure 11, it is graphically explained the process of local separator failure and its consequence involving the electrolyte and the adjacent layers.

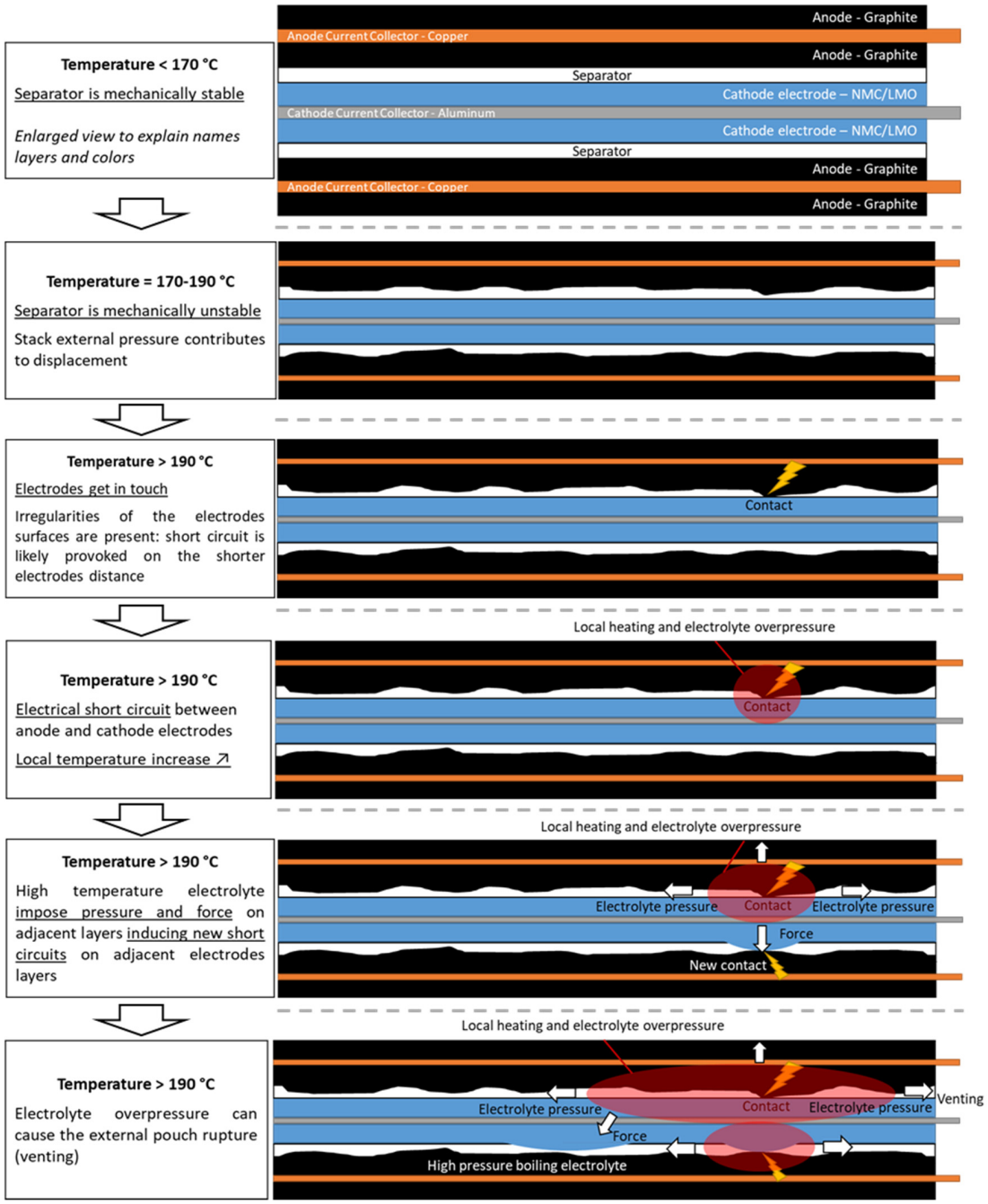

Figure 11. Description of expected internal phenomena occurring during initial warming up phase and TR triggering. Temperature ranges refer to the DSC analysis and not to measured ones during TR propagation test. In fact, during experiment external temperature is measured while described processes are triggered by internal temperatures.

Once the separator fails in a precise location, this failure propagates, as explained in Figure 11. From the plot of Figure 8, it is possible to understand the speed of this internal short circuit propagation: within 15 s the voltage drops to zero and the temperature rises to about 700 °C. Furthermore, it is possible to deduct that the thermal runaway severity shows a dependency on the external force applied to the stack. Looking at the voltage drop of each cell (as illustrated in Figure 9), when TR occurs in the first cell the stack is loaded with the maximum pressure, as soon as the first cell is triggered and in deep TR, the thickness of the cell stack will be reduced lowering the stack pressure. Consequently, the successive cells will sustain different pressure when TR will be triggered. The effect of this phenomenon can be evaluated observing the time between the first voltage variation and the massive internal short circuit in Figure 9. In fact, the cell number two shows a longer initial discharge before to get into the massive short circuit condition, this variation gets higher and higher for next cells as it is visible for cells three and four.

From the postmortem inspection (as illustrated in Figure 10), the path of the electrical short circuit propagation on single cell level is visible, and the propagation is provoked by the overpressure of the electrolyte in the area of the first short circuit.

On module level, the propagation cell-to-cell can be evaluated observing the temperatures or the voltages. Since the internal separator failure of a cell is the precursor of massive internal short circuit and TR, the voltage drop reveals the very first cell failure. Since thermocouples cannot be placed on the inner material of the cell, the measured temperature will not be a precise indicator of the TR event. This time discrepancy is explained in Figure 8, where voltage and temperature relative to one cell are compared. For this reason, the time intervals of TR propagation, reported in Table 2, are based on cells' voltage drop.

5. Conclusions

The presented work gives insights about thermal runaway (TR) process in terms of electrical and thermal behavior in a Li-ion batteries module. A stack of four commercial Li-ion cells were triggered to TR—by overheating the first cell of the stack—and the evolution observed by voltage and temperature sensors. The information about TR propagation timing is of great interest since the Global Transport Regulation [1] defines a minimum time window of 5 min in between the first TR event and a hazardous situation inside the passenger compartment. In this manuscript, more insights about the timing and TR process were provided reporting temperatures, voltages, visible effects, and postmortem inspection. Eight distinct phases were identified by observing five repetition tests conducted on equivalent samples at 100% SOC and in same testing conditions. Furthermore, physical meaning of the observed effects were hypothesized for each phase in the respective temperature range, and an ideal illustration was provided of what is expected to take place on single cell level. The provided assumptions could be particularly useful for the implementation of finite element models and computational fluid dynamics simulations of the TR process as well as from electric and thermodynamic perspectives. From the results and postmortem inspection, the electrolyte seems to play an important role on the propagation speed of the electrical short circuit on single cell level due to the increase of pressure as consequence of the increase of temperature. The provided data could be useful to predict, for example, the gas venting point on the pouch bag in case of TR condition. Furthermore, voltage and temperatures can be useful for the electrothermal simulation validation of TR process. For future test improvements, it could be of great interest to measure the pressure of the stack during the whole experimental procedure.

Author Contributions: Conceptualization, L.A.; Data curation, L.A.; Investigation, L.A.; Methodology, L.A.; Project administration, C.E. and W.S.; Supervision, W.S.; Visualization, L.A.; Writing—original draft, L.A.; Writing—review & editing, L.A., I.H., G.G., E.E. and W.S. All authors have read and agreed to the published version of the manuscript.

Funding: This work origins from the research project SafeBattery (grant no. 856234). The K-project SafeBattery is funded by the federal ministry for transport, innovation, and technology (BMVIT), federal ministry of digital and economic affairs (BMDW), Austria and Land Styria within the program COMET—Competence Centers for Excellent Technologies. The program COMET is administered by the FFG. This work was also based on the research project SafeLIB (grant no. 882506). The K-project SafeLIB is funded by the Austrian federal ministry for climate action, environment, energy, mobility innovation and technology (BMK), federal ministry of digital and economic affairs (BMDW), the provinces Styria and Upper Austria within the program COMET—Competence Centers for Excellent Technologies. The program COMET is administered by the FFG.

Institutional Review Board Statement: Not applicable.

Data Availability Statement: The whole data of interest was included thanks to the Appendix A.

Acknowledgments: We would like to thank all our colleagues from VSI and ICTM institutes for the teamwork and effort put into reaching the objectives. The targets were achieved thanks to the valuable input of the consortium members of the SafeBattery project. "Open Access Funding by the Graz University of Technology".

Conflicts of Interest: The authors declare no conflict of interest.

Appendix A

The following Figures A1 and A2 shows the temperature measurements and voltage measurements of modules 2, 3, 4, 5.

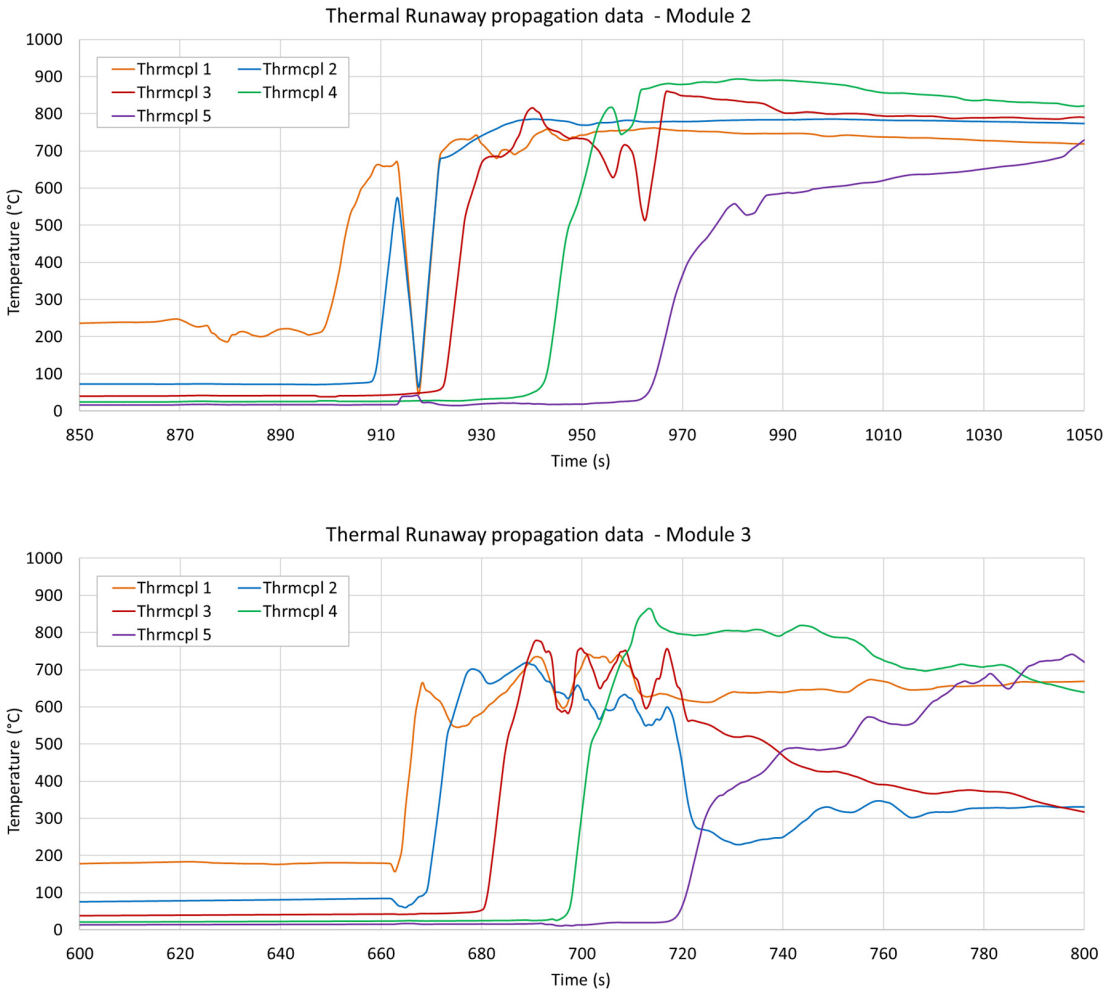

Figure A1. *Cont.*

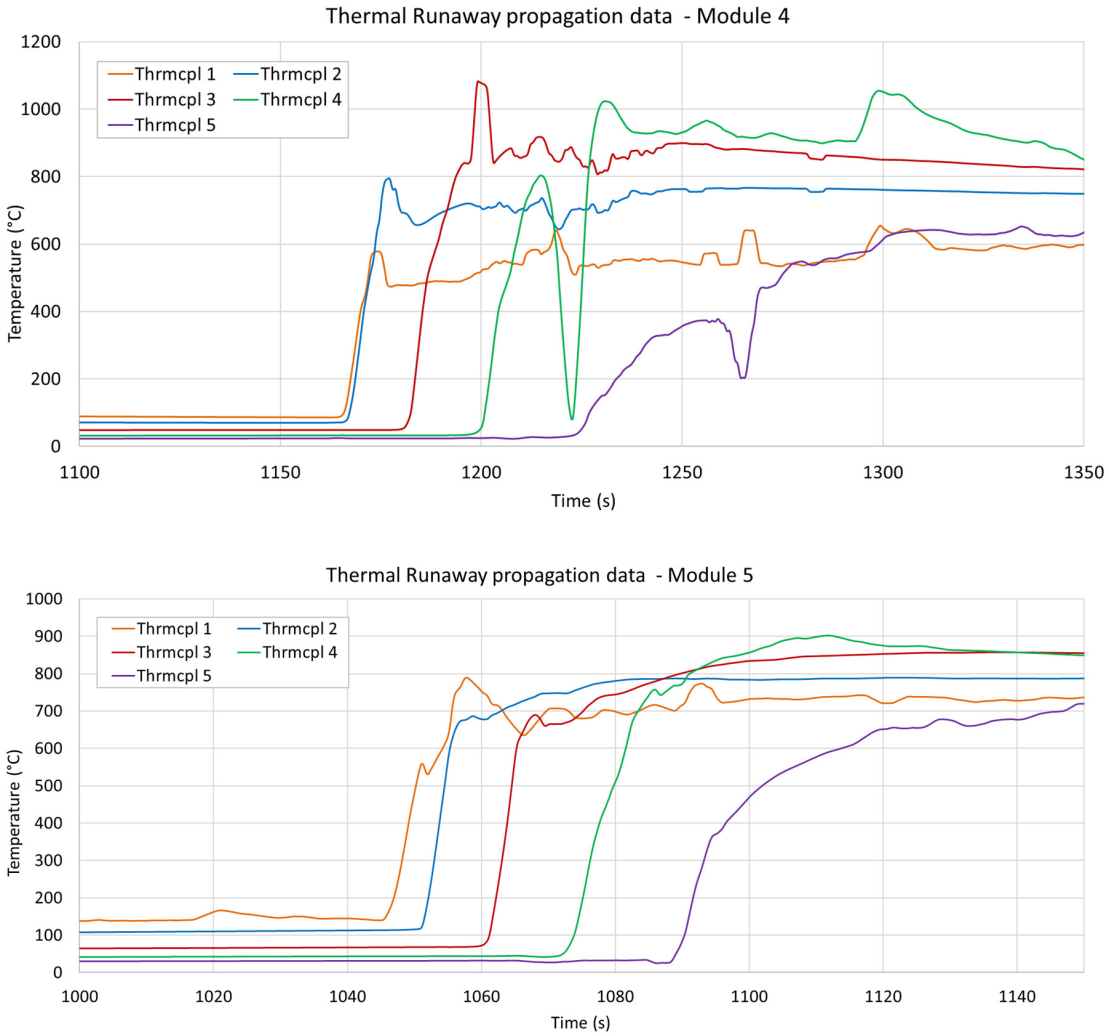

Figure A1. Temperature measurements of modules 2, 3, 4, 5.

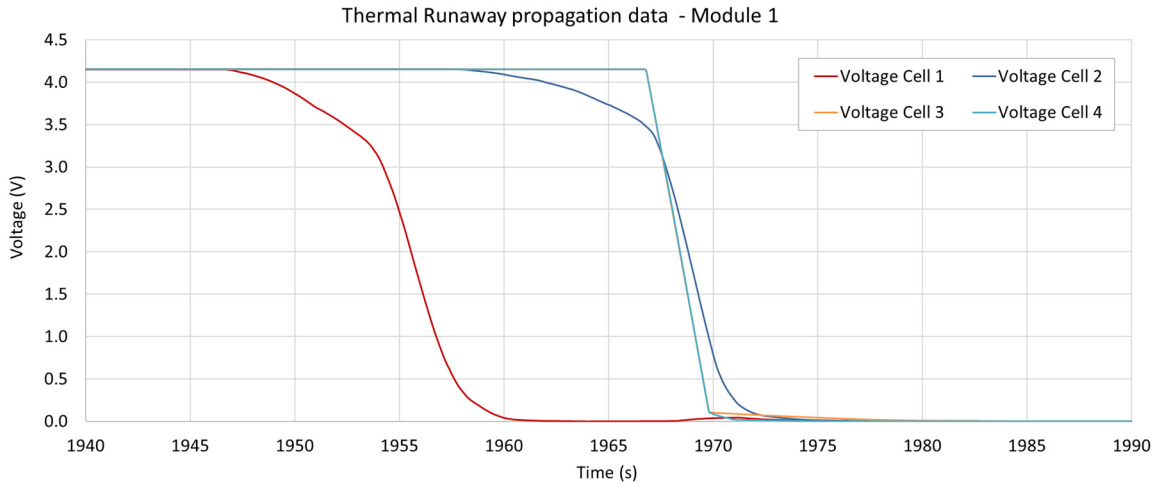

Figure A2. *Cont*.

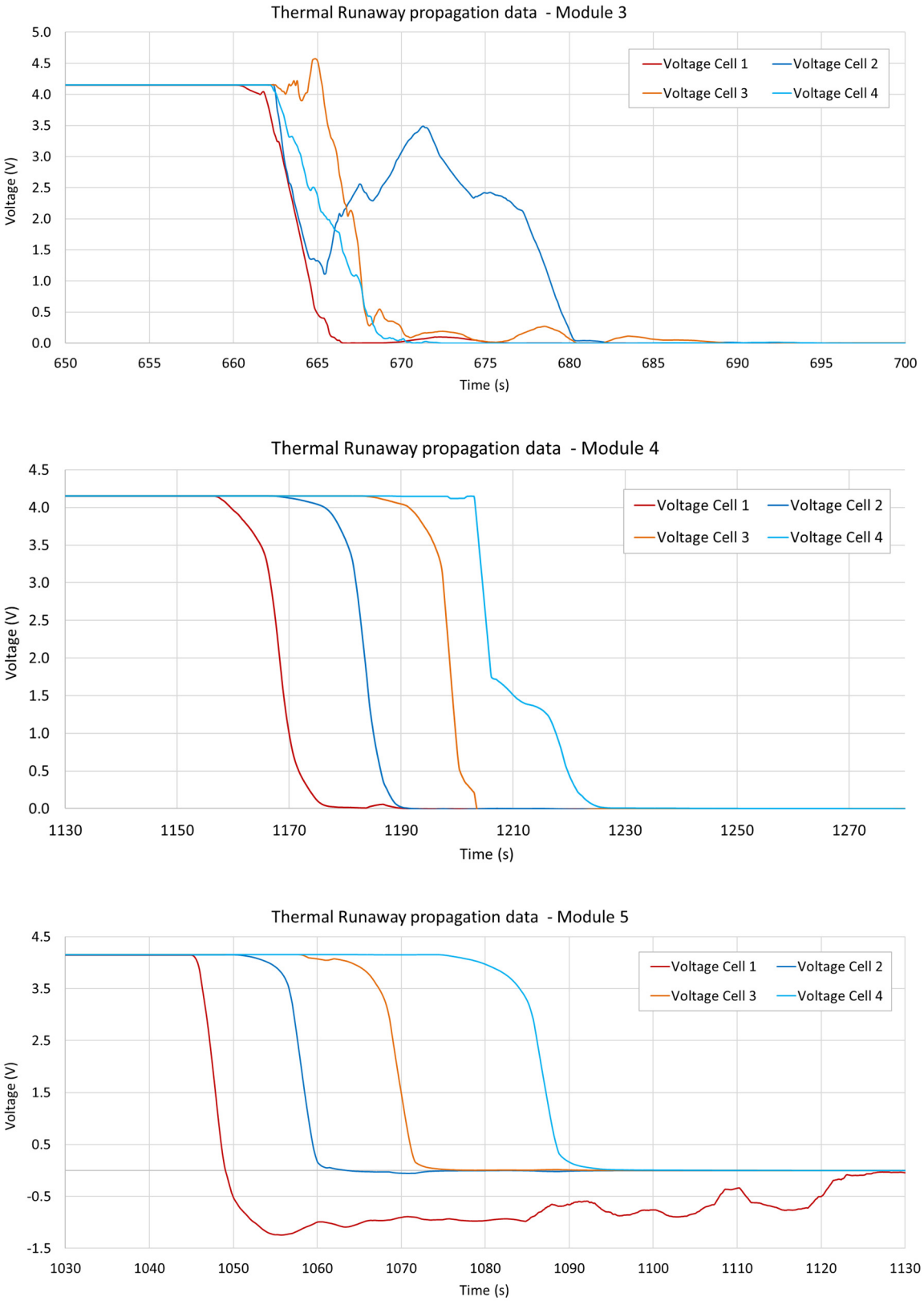

Figure A2. Voltage measurements of modules 1,3,4,5.

References

1. Global Registry. Global Technical Regulation on the Electric Vehicle Safety (EVS), ECE-United Nations. 2018. Available online: https://unece.org/ (accessed on 31 March 2021).
2. Baird, A.R.; Archibald, E.J.; Marr, K.C.; Ezekoye, O.A. Explosion hazards from lithium-ion battery vent gas. *J. Power Sources* **2020**, *446*, 227257. [CrossRef]
3. Feng, X.; Zheng, S.; Ren, D.; He, X.; Wang, L.; Cui, H.; Liu, X.; Jin, C.; Zhang, F.; Xu, C.; et al. Investigating the thermal runaway mechanisms of lithium-ion batteries based on thermal analysis database. *Appl. Energy* **2019**, *246*, 53–64. [CrossRef]
4. Feng, X.; Ouyang, M.; Liu, X.; Lu, L.; Xia, Y.; He, X. Thermal runaway mechanism of lithium ion battery for electric vehicles: A review. *Energy Storage Mater.* **2018**, *10*, 246–267. [CrossRef]
5. Lei, B.; Zhao, W.; Ziebert, C.; Uhlmann, N.; Rohde, M.; Seifert, H.J. Experimental Analysis of Thermal Runaway in 18650 Cylindrical Li-Ion Cells Using an Accelerating Rate Calorimeter. *Batteries* **2017**, *3*, 14. [CrossRef]
6. Mao, B.; Huang, P.; Chen, H.; Wang, Q.; Sun, J. Self-heating reaction and thermal runaway criticality of the lithium ion battery. *Int. J. Heat Mass Transf.* **2020**, *149*, 119178. [CrossRef]
7. Mukai, T.; Sakai, T.; Yanagida, M. Thermal Runaway Mechanism and High Safety Technology of Lithium Ion Battery. *J. Surf. Finish. Soc. Jpn.* **2019**, *70*, 301–307. [CrossRef]
8. Zhong, G.; Mao, B.; Wang, C.; Jiang, L.; Xu, K.; Sun, J.; Wang, Q. Thermal runaway and fire behavior investigation of lithium ion batteries using modified cone calorimeter. *J. Therm. Anal. Calorim.* **2019**, *135*, 2879–2889. [CrossRef]
9. Cheng, X.; Li, T.; Ruan, X.; Wang, Z. Thermal Runaway Characteristics of a Large Format Lithium-Ion Battery Module. *Energies* **2019**, *12*, 3099. [CrossRef]
10. Feng, X.; Fang, M.; He, X.; Ouyang, M.; Lu, L.; Wang, H.; Zhang, M. Thermal runaway features of large format prismatic lithium ion battery using extended volume accelerating rate calorimetry. *J. Power Sources* **2014**, *255*, 294–301. [CrossRef]
11. Li, H.; Chen, H.; Zhong, G.; Wang, Y.; Wang, Q. Experimental study on thermal runaway risk of 18650 lithium ion battery under side-heating condition. *J. Loss Prev. Process. Ind.* **2019**, *61*, 122–129. [CrossRef]
12. Wang, Z.; Yang, H.; Li, Y.; Wang, G.; Wang, J. Thermal runaway and fire behaviors of large-scale lithium ion batteries with different heating methods. *J. Hazard. Mater.* **2019**, *379*, 120730. [CrossRef] [PubMed]
13. Kriston, A.; Kersys, A.; Antonelli, A.; Ripplinger, S.; Holmstrom, S.; Trischler, S.; Döring, H.; Pfrang, A. Initiation of thermal runaway in Lithium-ion cells by inductive heating. *J. Power Sources* **2020**, *454*, 227914. [CrossRef]
14. Feng, X.; He, X.; Ouyang, M.; Lu, L.; Wu, P.; Kulp, C.; Prasser, S. Thermal runaway propagation model for designing a safer battery pack with 25Ah LiNixCoyMnzO2 large format lithium ion battery. *Appl. Energy* **2015**, 74–91. [CrossRef]
15. Huang, P.; Ping, P.; Li, K.; Chen, H.; Wang, Q.; Wen, J.; Sun, J. Experimental and modeling analysis of thermal runaway propagation over the large format energy storage battery module with $Li_4Ti_{15}O_{12}$ anode. *Appl. Energy* **2016**, *183*, 659–673. [CrossRef]
16. Larsson, F.; Anderson, J.; Andersson, P.; Mellander, B.-E. Thermal Modelling of Cell-to-Cell Fire Propagation and Cascading Thermal Runaway Failure Effects for Lithium-Ion Battery Cells and Modules Using Fire Walls. *J. Electrochem. Soc.* **2016**, *163*, A2854–A2865. [CrossRef]
17. Said, A.O.; Lee, C.; Stoliarov, S.I.; Marshall, A.W. Comprehensive analysis of dynamics and hazards associated with cascading failure in 18650 lithium ion cell arrays. *Appl. Energy* **2019**, *248*, 415–428. [CrossRef]
18. Tao, C.; Li, G.; Zhao, J.; Chen, G.; Wang, Z.; Qian, Y.; Cheng, X.; Liu, X. The investigation of thermal runaway propagation of lithium-ion batteries under different vertical distances. *J. Therm. Anal. Calorim.* **2020**, *155*, 401. [CrossRef]
19. Wang, Z.; Mao, N.; Jiang, F. Study on the effect of spacing on thermal runaway propagation for lithium-ion batteries. *J. Therm. Anal. Calorim.* **2019**, *10*, 430. [CrossRef]
20. Sun, L.; Wei, C.; Guo, D.; Liu, J.; Zhao, Z.; Zheng, Z.; Jin, Y. Comparative Study on Thermal Runaway Characteristics of Lithium Iron Phosphate Battery Modules Under Different Overcharge Conditions. *Fire Technol.* **2020**, *3*, 43. [CrossRef]
21. Huang, L.; Zhang, Z.; Wang, Z.; Zhang, L.; Zhu, X.; Dorrell, D.D. Thermal runaway behavior during overcharge for large-format Lithium-ion batteries with different packaging patterns. *J. Energy Storage* **2019**, *25*, 100811. [CrossRef]
22. Wang, Z.; Liu, K.; Liu, J.; Luo, Q.; Ma, C. Influence of the charging and discharging of the 18650 lithium-ion battery thermal runaway. *J. Loss Prev. Process. Ind.* **2017**. [CrossRef]
23. Ma, X.; Zhu, C.; Xie, Z.; Xie, C.; Wang, W.; Zheng, J.; Mu, D.; Wu, B. Progress in Thermal Modeling for Lithium-ion Battery. *DEStech Trans. Environ. Energy Earth Sci.* **2019**. [CrossRef]
24. Gao, T.; Wang, Z.; Chen, S.; Guo, L. Hazardous characteristics of charge and discharge of lithium-ion batteries under adiabatic environment and hot environment. *Int. J. Heat Mass Transf.* **2019**, *141*, 419–431. [CrossRef]
25. Liu, X.; Stoliarov, S.I.; Denlinger, M.; Masias, A.; Snyder, K. Comprehensive calorimetry of the thermally-induced failure of a lithium ion battery. *J. Power Sources* **2015**, *280*, 516–525. [CrossRef]
26. Golubkov, A.W.; Scheikl, S.; Planteu, R.; Voitic, G.; Wiltsche, H.; Stangl, C.; Fauler, G.; Thaler, A.; Hacker, V. Thermal runaway of commercial 18650 Li-ion batteries with LFP and NCA cathodes—Impact of state of charge and overcharge. *RSC Adv.* **2015**, *5*, 57171–57186. [CrossRef]
27. Spotnitz, R.M.; Franklin, J. Abuse behavior of high-power, lithium-ion cells. *J. Power Sources* **2003**, *113*, 81–100. [CrossRef]
28. Kovachev, G.; Schröttner, H.; Gstrein, G.; Aiello, L.; Hanzu, I.; Wilkening, H.M.R.; Foitzik, A.; Wellm, M.; Sinz, W.; Ellersdorfer, C. Analytical Dissection of an Automotive Li-Ion Pouch Cell. *Batteries* **2019**, *5*, 67. [CrossRef]